The *Euclid* mission: status after launch and early operations

R. Laureijs*[1], R. Vavrek[2], G. D. Racca[1], R. Kohley[2], P. Ferruit[2], V. Pettorino[1], T.-Bönke[1], A. Calvi[1], L. Gaspar Venancio[1], L. Campos[1], E. Maiorano[1], O. Piersanti[1], S. Prezelus[1], U. Ragnit[1], P. Rosato[1], C. Rosso[1], H. Rozemeijer[1], A. Short[1], P. Strada[1], D. Stramaccioni[1], M. Szafraniec[1], B. Altieri[2], G. Buenadicha[2], X. Dupac[2], P. Gómez Alvarez[2], K. Henares Vilaboa[2], C. Hernandez de la Torre[2], J. Hoar[2], M. Lopez-Caniego Alcarria[2], P. Marcos Arenal[2], J. Martín Fleitas[2], M. Miluzio[2], A. Mora[2], S. Nieto[2], R. Perez Bonilla[2], P. Teodoro Idiago[2], F. Cordero[3], J. Mendes[3], F. Renk[3], A. Rudolph[3], M. Schmidt[3], J. Schwartz[3], Y. Mellier[4, 15], H. Aussel[4], M.-Berthé[4], P. Casenove[8], M. Cropper[5], J. C. Cuillandre[4], J. Dinis[6, 21], A. Gregorio[9], K. Kuijken[14], T. Maciaszek[8], L. Miller[16], R. Scaramella[7], M. Schirmer[10], I. Tereno[6], A. Zacchei[13], S. Awan[5], G.P. Candini[5], P. Liebing[5], R. Nakajima[11], S. Dusini[12], P. Battaglia[20], E. Medinacelli[20], C. Sirignano[12], I. Baldry[27], C. Baugh[26], F. Bernardeau[15], F. Castander[17], A. Cimatti[19], W. Gillard[18], L. Guzzo[22], H.-Hoekstra[14], K. Jahnke[10], T. Kitching[5], J. E. Martin[28], J.J. Mohr[23], W. Percival[24], J. Rhodes[25],
on behalf of the *Euclid Collaboration*

[1]European Space Agency / ESTEC, Keplerlaan 1, 2201 AZ Noordwijk, The Netherlands
[2]European Space Agency / ESAC, Villanueva de la Cañada, E-28692 Madrid, Spain
[3]European Space Agency / ESOC, Robert-Bosch-Str. 5, 64293 Darmstadt, Germany
[4]Univ. Paris-Saclay, Univ. Paris Cité, CEA, CNRS, AIM, 91191, Gif-sur-Yvette, France
[5]MSSL, University College London, Holmbury St Mary, Dorking, Surrey RH5 6NT, UK
[6]FCUL, Univ. de Lisboa, Edificio C8, Campo Grande, 1749-016 Lisboa, Portugal
[7]INAF-Osservatorio di Roma, Via Frascati 33, 00040 Monteporzio Catone (Roma), Italy
[8]CNES, 18 avenue Edouard Belin, F-31401 Toulouse Cedex 9, France
[9]Dept of Physics, Univ. Trieste, Via Valerio 2, 34127 Trieste, Italy
[10]Max Planck Institute for Astronomy, Koenigstuhl 17, D-69117, Heidelberg, Germany
[11]Argelander-Institut für Astronomie, Auf dem Hügel 71, 53121 Bonn, Germany
[12]INFN, Dept. of Physics and Astronomy, Univ. Padova, via Marzolo 8, 35131 Padova, Italy
[13]INAF-Osservatorio di Trieste, Via G.B. Tiepolo 11, 31131 Trieste, Italy
[14] Leiden Observatory, Leiden Univ., Einsteinweg 55, 2333CA Leiden, The Netherlands
[15]CNRS-UPMC, Institut d'Astrophysique de Paris, 98B Bd Arago, F-75014 Paris, France
[16]Dept. of Physics, Univ. Oxford, Keble Road, Oxford, OX1 3RH, UK
[17]IEEC, UAB, Gran Capita 2-4, 08034 Barcelona, Spain
[18]CPPM, Aix-Marseille Univ, Ave. de Luminy, 13009 Marseille, France
[19]Dipartimento di Fisica e Astronomia, Univ. Bologna, Via Gobetti 93/2, 40126 Bologna, Italy
[20]INAF-OAS, Via Gobetti 93/3, 40129 Bologna, Italy
[21]IACE, Faculdade de Ciências, Univ. de Lisboa, Campo Grande, 1749-016 Lisboa, Portugal
[22]Dipartimento di Fisica, Univ. Milano, Via Celoria 16, 20133 Milan, Italy
[23]University Observatory, LMU Faculty of Physics, Scheinerstrasse 1, 81679 Munich, Germany
[24]WCA, Univ. of Waterloo, Waterloo, Ontario, N2L 3G1, Canada
[25]JPL/NASA, 4800 Oak Grove Dr., Pasadena, CA91109 USA
[26]ICC, Department of Physics, Durham Univ., South Road, Durham DH1 3LE, UK
[27]ARI, Liverpool John Moores Univ., 146 Brownlow Hill, Liverpool L3 5RF, UK
[28]IAC, c/Via Lactea, s/n E38205 La Laguna, Tenerife, Spain

Space Telescopes and Instrumentation 2024: Optical, Infrared, and Millimeter Wave, edited by Laura E. Coyle, Shuji Matsuura, Marshall D. Perrin, Proc. of SPIE Vol. 13092, 130920M · © 2024 SPIE · 0277-786X · doi: 10.1117/12.3020343

ABSTRACT

During its 6-year nominal mission, *Euclid* shall survey one third of the sky, enabling us to examine the spatial distributions of dark and luminous matter during the past 10 Gyr of cosmic history. The *Euclid* satellite was successfully launched on a SpaceX Falcon 9 launcher from Cape Canaveral on 1 July 2023 and is fully operational in a halo orbit around the Second Sun-Earth Lagrange point. We present an overview of the expected and unexpected findings during the early phases of the mission, in the context of technological heritage and lessons learnt. The first months of the mission were dedicated to the commissioning of the spacecraft, telescope and instruments, followed by a phase to verify the scientific performance and to carry out the in-orbit calibrations. We report that the key enabling scientific elements, the 1.2-meter telescope and the two scientific instruments, a visual imager (VIS) and a near-infrared spectrometer and photometer (NISP), show an in-orbit performance in line with the expectations from ground tests. The scientific analysis of the observations from the Early Release Observations (ERO) program done before the start of the nominal mission showed sensitivities better than the pre-launch requirements. The nominal mission started in December 2023, and we allocated a 6-month early survey operations phase to closely monitor the performance of the sky survey. We conclude with an outlook of the activities for the remaining mission in the light of the in-orbit performance.

Keywords: *Euclid*, space telescope, cosmology, galaxies survey, mission performance, data processing

1. INTRODUCTION

The *Euclid* mission provides a Stage IV dark energy survey as defined in [1], and it is expected to improve the dark energy figure of merit by an order of magnitude compared to Stage II surveys. The 6-year nominal mission has been optimized for the Weak Lensing (WL) and Galaxy Clustering (GC) dark energy probes, and the science requirements demand a space-based survey in the visual and near-infrared from 0.550 to 2 micron, complemented by ground-based photometry in at least 4 optical bands (*g*, *r*, *i*, *z*) for the WL galaxies over the entire survey area. The *Euclid* mission must provide a sky survey of 14000 deg^2 and shall yield the precise shapes and photometric redshifts with an accuracy of $\Delta z/(z+1) < 5\%$ for 30 galaxies per arcmin^2 on average for WL, and spectroscopic redshifts with an accuracy better than $\Delta z/(z+1) < 0.1\%$ for more than 1700 galaxies per deg^2 for GC [2].

Equipped with a 1.2 m telescope for diffraction-limited imaging in the visual as well as photometry and spectroscopy in the near-infrared, *Euclid* will provide a 3-dimensional map showing cosmic structures with redshift *z* as the third dimension, which corresponds to light travel time. For the construction of the atlas, *Euclid* will measure more than 1.5 billion galaxies for the WL probe and 20–30 million galaxies with spectroscopic redshifts for the GC probe. A comprehensive description of the scientific objectives and expected results of the *Euclid* mission based on the pre-launch performance can be found in [3].

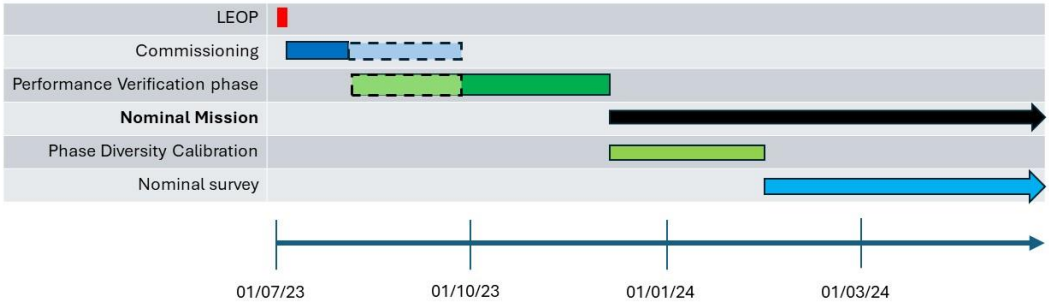

Figure 1: Early phases of the Euclid operations after launch on 1 July 2023: the nominal mission started on 3 December 2023 with a two-month phase-diversity calibration period to determine the telescope wavefront error for the construction of a detailed PSF model, before the start of the nominal survey in February 2024. The dashed areas indicate the period where the guiding was not reliable.

The *Euclid* mission is developed and operated by the European Space Agency (ESA) [4]. The Euclid Consortium (EC) provided the scientific instruments and is responsible for the operation and maintenance of the instruments, the provision of the survey plan, and the scientific data processing and analysis including the delivery of the data products. During all mission phases the EC is closely collaborating with ESA to ensure that the scientific performance can meet the science

objectives of the mission. *Euclid* consists of a space segment with a payload module (PLM) designed and developed by Airbus Defence and Space, Toulouse, France, containing the telescope and the two EC provided scientific instruments, the visual imaging instrument VIS [5] and the near-infrared spectrometer and photometer NISP [6], and a service module (SVM) designed and developed by Thales Alenia Space, Torino, Italy, containing the warm electronics of the instruments and the standard spacecraft subsystems. The ground segment consists of the *Euclid* Mission Operations Centre (MOC) in ESOC Darmstadt, Germany, the *Euclid* Science Operations Centre (SOC) in ESAC Madrid, Spain, and the Science Ground Segment (SGS) for the generation of the scientific data products. The EC led SGS is distributed over 8 science data centers (SDCs) in Europe and one in the US. During *Euclid's* study and development phases, technical status reports to the SPIE were provided of the mission and the individual instruments; we refer to the latest pre-launch descriptions and references therein [4], [7], [8].

After launch, the mission timeline consisted of the following periods: (1) launch and early operations phase (LEOP), (2) spacecraft commissioning phase, (3) performance verification (PV) phase, and the (4) nominal mission, see the timeline depicted in Fig. 1. The commissioning phase was extended by 7 weeks to resolve the guiding anomaly, see Section 6. During this extension period we could still collect PV measurements that do not involve pointing as well as observations of fields with sufficient guide stars for stable guiding. Driven by the WL science requirements, a dedicated in-orbit characterization of the point spread function (PSF) for the VIS imager was performed before the start of the nominal survey. The Euclid phase-diversity calibration (PDC) campaign lasted about two months until the start of the nominal survey.

The *Euclid* operations phase started on the first of July 2023 after a successful launch with a SpaceX Falcon 9 launcher from Cape Canaveral, Florida, USA. At the time of writing of these proceedings, we completed 1 year of operations. Like for other missions, we made a detailed planning for the early mission phases and for the entire Euclid survey based on the as-built expectations.

A review is presented of the first year of operations. We start with an overview of the heritage from other missions and the novel science-enabling elements in *Euclid*, followed by a description of the subsequent mission phases, including the anomalies we encountered. For the anomalies we discuss the mitigations and possible trade-offs for the optimization of the mission. We conclude with an outlook of the remainder of the mission.

2. HERITAGE AND LESSONS LEARNT FROM OTHER MISSIONS

The design of *Euclid* has important elements of heritage from other missions. This was the answer to the ESA Cosmic Vision program imposing M-class missions to use technologies with technology readiness level (TRL) of 5 or higher. Here we mention the science enabling key components used for *Euclid*, decided after trade-off studies.

Building on the successful application of SiC instrumentation in other ESA science missions such as Herschel, Gaia and JWST, it was decided to use SiC for the entire Korsch three mirror anastigmat (TMA) telescope assembly, base plate optical bench, and instrument elements to achieve a homothetic structural PLM design for *Euclid* [9]. The key properties of SiC are a high specific stiffness and high thermal stability. In combination with its high mechanical strength, the SiC material can be used for both telescope mirrors as well as structural parts.

Euclid uses a micro-propulsion system (MPS) with cold gas thrusters for the guiding actuation by the fine-guidance sensor, to meet the stringent relative pointing requirement. The choice of a cold gas MPS was based on the usage and in-orbit performance knowledge provided by LISA-pathfinder and Gaia.

The telescope focusing mechanism is also a heritage from Gaia. It supports the secondary mirror (M2) and can be actuated to adjust the position of M2. The original 5 degree of freedom (DoF) mechanism was simplified to a 3 DoF mechanism (piston and tip-tilt). The initial usage of the mechanism was to put the telescope in its final focus position directly after launch, but during the development phase it was proposed to repeatedly exercise the mechanism for dedicated wavefront error (WFE) measurements, see Section 8. This required an additional qualification of the mechanism and the allocation of the allowed settings for the WFE measurements.

The *Euclid* sensors have a strong heritage from both ground-based and space-based instrumentation. The *Euclid* CCD273-84 was optimized to minimize PSF degradation due to charge transfer inefficiency (CTI) because of radiation damage [10]. The effects of CTI on the data for science missions have been studied in detail, see e.g. [11]. CCD273 features a narrower serial register, a low-noise output stage, and a charge injection capability, taken from earlier CCD models offered by Teledyne-e2v [12]. The near-infrared H2RG detectors and electronics assemblies fabricated by Teledyne Imaging Systems

make use of the strong heritage from NASA missions [13]. The manufacturing of the *Euclid* H2RG model was optimized by imposing a long wavelength cut-off at 2.3 micron to avoid the detection of a noise component generated by the 150 K thermal radiation from the PLM, radiating just longward of 2.3 micron.

From Gaia two further lessons learnt were carried out. Once in orbit Gaia showed that there was a source of unexpected straylight, which likely originated by filaments sticking off the edges of the sunshield made of multi-layer insulation (MLI) foils with fabric polyester spacers. These filaments can diffract sunlight into the telescope. Furthermore, a rather high content of water ice was detected affecting the throughput of the telescope. Gaia had planned to dispose of the water ice by heating the cold parts of the telescope that were trapping the ice by heaters but did not consider to use Solar illumination to heat up the relevant parts.

Euclid was designed with these two lessons learnt in mind, considering that its sensitivity to both ice contamination and straylight is higher than Gaia's. The Euclid sunshield top edge with view into the telescope baffle is endowed with a three blades linear baffle (see Fig. 2) to reduce the possible sunlight diffraction. Calculation performed following the theory of Fresnel diffraction at a straight edge showed that the flux reduction calculated for this configuration was about 2×10^{-16}, which was largely meeting the required performance, which was an attenuation better than 10^{-10}. All other surfaces and edges on the spacecraft are not considered optical elements, they are away from the telescope field of view.

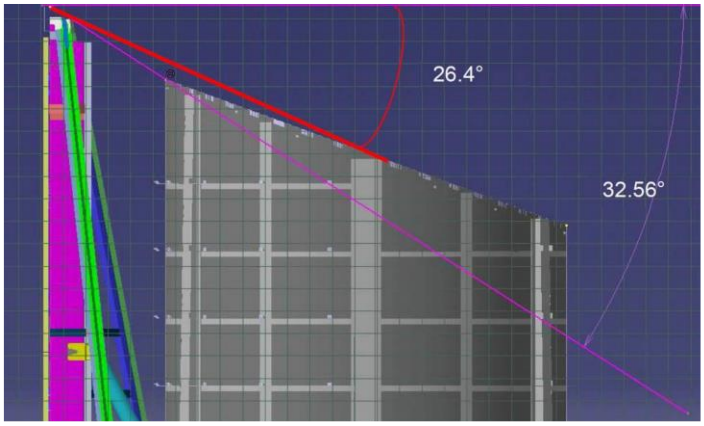

Figure 2 The configuration of the 3-blade baffle of the sunshield

The amount of water was minimized by design and construction in the PLM. The PLM itself was separated by the SVM by means of two sets of MLI blankets. One MLI blanket composed of 22 Mylar layers sandwiched between one Kapton and one thicker Mylar layer, and one 13-layer MLI blanket on the PLM side in addition to a single layer foil of 1.6 mil Kapton, aluminized on the PLM side to prevent contamination between the SVM and the PLM. This single layer insulation is supported by a dedicated net attached to the PLM/SVM 6 struts fittings. Apart from contamination, the double PLM/SVM MLI insulation minimizes radiative heat-load from the SVM on the PLM.

Eventually, even if minimized, the water content of the PLM will deposit at low temperatures reached in orbit on the cold surfaces and needs to be removed. To this aim, all the optical surfaces have heaters applied in their back (such as the reflectors) or in the vicinity of their active surfaces (such as the dichroic). However other non-optical surfaces that could also trap water ice would be difficult to heat by electric heaters. Therefore, *Euclid* was designed to support a decontamination mode attitude, that would allow the telescope axis to be tilted towards the Sun direction to a Solar aspect angle (SAA = the angle between the telescope pointing direction and the direction to the center of the Solar disk) up to 45º, while the maximum tolerated SAA during nominal operations is 87 to 121 deg. The resulting global decontamination procedure was exercised during the spacecraft commissioning and could be exercised again during the mission if needed (see also lessons learnt in Section 10).

3. NOVEL ELEMENTS IN *EUCLID*

Euclid is the first ESA science mission making use of 26 GHz K-band communications for the downlink of science data from the second Sun-Earth Lagrange orbit. The K-band transponder transfers about 1 Tbit of the science data to ground during the allocated 4 hours of daily contact. The ESA deep space network (ESTRACK) with antennas in Cebreros (Spain),

Malargüe (Argentina) and New Norcia (Australia) had to be equipped with K-band receivers to support the *Euclid* mission. *Euclid* is the first ESA satellite using a new data transfer protocol using the CCSDS File Delivery Protocol (CFDP) [7].

To minimize micro-vibrations below 1 Hz, the satellite will stop spinning its reaction wheels during the science exposures. Studies showed that this was the only viable solution to meet the pointing stability requirement of 25 (3 sigma) milli-arcsec (mas) in 700 s, imposed by the image quality requirements for the WL probe. The reaction wheels are used for slewing between fields, the guiding during exposures is governed by the FGS with cold gas thruster actuators. A dedicated qualification program for the reaction wheels had to be carried out to ensure the TRL level before adoption. This qualification was also necessary for the compensating movement unit (CMU). The CMU is a spacecraft system mounted in the SVM to compensate for the torques generated by the grism and filter wheel actuations by NISP in the PLM.

The FGS is a novel subsystem developed by industry for an ESA science mission. It uses the industrial heritage of satellite star trackers in Europe. Due to the pointing requirements for the tiling of the survey fields, the FGS has the capability to carry out an absolute pointing using catalogued stars. The *Euclid* FGS star catalogue has been derived from the Gaia DR1 star catalogue, and the flight operations include the uplink of subsets of the FGS star catalogue to support the identification of guide stars near the survey fields.

During the development phase, it was found that the many dielectric layers needed to define the VIS bandpass in the VIS focal plane can cause unaccounted interferences which can change the shape of the bandpass [14]. This has led to the replacement of the dielectric coating of the flat optical mirror (FOM) 3 with reflective silver coating. A test bench was developed to measure the wavefront error of the dichroic mirror as function of wavelength, polarization, and position on the mirror [15]. The development of the test bench was completed in December 2023. The measurements are performed with the qualification model of the dichroic mirror assuming sufficient similarity with the flight model for which an identical production process was applied. The data will be necessary input for the most accurate optical model used to fit the broadband PSF model applicable to WL galaxies.

4. LAUNCH WITH SPACE X FALCON 9

Shortly after the start of the war in Ukraine, Roscosmos decided in February 2022 to withdraw its workforce from ESA spaceport Centre Spatial Guyanais (CSG) in French Guiana. This caused a serious problem for the *Euclid* mission because the baseline was a launch with the Soyuz ST-B with a Fregat MT upper stage combination from CSG, with an assumed launch period in the second quarter of 2023. The backup launcher would have been an Ariane 6 with two solid boosters (A62). There were no technical showstoppers for the utilization of A62, but the mechanical compatibility had to be confirmed and most likely a passive isolation device (PID) was required to create a mechanical environment compatible with a Soyuz launcher combination, which is typically more benign than many other launch vehicles. However, the A62 development schedule did not allow an A62 launch opportunity before late 2024 and the risk of further delay was unquantified. Such a delay would seriously affect the continuity of the available expertise and workforce. In addition, the science community argued that an earlier *Euclid* launch would be highly preferred from a scientific perspective in view of the upcoming Dark Energy Stage IV surveys.

Assessment of a few available launcher candidates indicated that the SpaceX Falcon 9 rocket would be the most suitable alternative considering the mission analysis, mechanical, and electrical criteria. Coupled loads analysis and analysis of actual flight data obtained from the numerous previous Falcon 9 launches showed that there was no need for a PID. An adaptation of the environmental tests at TAS-F in Cannes (held in February 2023) was required for the qualification of the mechanical compatibility of the satellite with the launcher base-driven random vibration environment. A low-level random test on the spacecraft flight model was performed and the transfer functions to the critical units were computed. An extrapolation of random levels at the interface of the units showed that the levels were covered by the existing qualifications at unit and subsystem level. Special attention was given to the cleanliness requirements demanding ISO5 in the fairing, together with N_2 purging and ISO-7 conditions in the encapsulation hall. This led to the usage of a new (i.e. not used in previous launches as customary with SpaceX) fairing procurement and encapsulation activities at Astrotech in Titusville. The negotiations with SpaceX resulted in an agreed launch in the third quarter of 2023, which eventually led to a very successful launch from Cape Canaveral launch complex 40 on the 1st of July 2023.

5. LAUNCH AND EARLY OPERATIONS AND SPACECRAFT COMMISSIONING PHASES

The launch of the spacecraft was successful, and the initial check-out of the subsystems showed that the *Euclid* spacecraft performed nominally after separation from the Falcon 9's upper stage. The launch and early operations phase lasted for

two days, with a first trajectory correction maneuver (TCM1) on day 2. The correction was modest due to an accurate orbit injection by the launcher. The performance of the operations ground segment was fully nominal.

The subsequent Spacecraft Commissioning Phase was planned to last 30 days, while *Euclid* was on a 30-day cruise to its halo orbit around the second Sun-Earth Lagrange point. During this phase two trajectory correction maneuvers (TCM2 and TCM3) were planned, but it was decided to skip TCM2 on day 7 because no correction was needed. The commissioning activities during this phase were driven by the industrial prime contractor (Thales Alenia Space, Italy). The first 10 days were dedicated to the decontamination procedure, which started by putting the spacecraft in its decontamination attitude of 51 deg from the Sun for a period of 4 days, as explained above. In the remaining 6 day cool down and stabilization period, other spacecraft systems were commissioned. During this time *Euclid*'s high-gain antenna (HGA) was successfully commissioned. The HGA is the only subsystem in the service module with an active mechanism.

The two scientific instruments were successfully activated, all instrument mechanisms, sensors, and electronics were working nominally. The telescope was subsequently put in focus with the aid of the imaging capabilities of the VIS instrument. The focusing was accomplished by adjusting M2 equipped with a 3 DoF focusing mechanism. Before launch, the mechanism was set in launch position, meaning that each actuator was set within a range compatible with the launch constraints. Thanks to the expertise provided by the PLM contractor (Airbus Defence and Space, France) a very accurate correction for the M2 piston and tilt could be predicted from the post-launch image. This correction was close to the final focus configuration of the telescope, which is the median solution over the field of view, and meeting the stringent image quality requirements for ellipticity, full width at half maximum (FWHM), and R^2. The focusing exercise confirmed the in-orbit performance of the telescope PSF, extensively tested on ground under 1-G conditions [8][19].

At the end of the nominal spacecraft commissioning phase, all subsystems were operational and redundant systems were successfully checked; no spacecraft hardware anomalies were found. Nevertheless, the scientific instruments registered anomalies that could seriously affect the scientific performance of the mission.

6. ANOMALIES FOUND DURING COMMISSIONING.

6.1 Parasitic straylight detected by VIS

The first images obtained by VIS both with closed and open shutter showed a higher and inhomogeneous background level. The features detected in the VIS images could be traced to mechanical structures in the instrument cavity of the PLM. The NISP instrument was not affected. The unexpected illumination was attributed to the presence of parasitic light not coming from the telescope aperture. It was quickly noticed that the parasitic straylight level depends on the spacecraft attitude, significantly disappearing for azimuth angles (denoted by α-angle or AA) less than −2.5 deg, and becoming detectable again at high elevation angles (Solar aspect angles SAA). A mapping of the VIS background on a grid of allowed AA and SAA angles showed that operations within a limited range of AA and SAA angles would yield VIS images with negligible parasitic straylight and meeting the image quality requirements, see Fig. 3. It was decided that the *Euclid* mission can continue but operating with the new AA and SAA constraints. There is, however, an impact on the total survey area, which will be described in Section 10.

The sharp decrease in straylight level below AA = −2.5 degrees can be associated with the transition of one of the spacecraft cold gas thruster booms moving into the shade of the sunshield. This suggests that the head of the boom illuminated by the Sun is reflecting sunlight to the back of the sunshield which has reflecting multi-layer insulation. A reflection is then entering the PLM cavity via some kind of opening in the PLM MLI blankets. The MLI blankets were designed and manufactured to be completely closed, although a real light tightness requirement was not specified. Calculations show that the MLI of typically more than 20 layers do block the light that is transmitted by the residual transparency of the single layers by a large factor. The joints and the attachment of the blankets are locally sewed or stapled and are covered by tape pieces on both sides of the blanket. The luminosity of the parasitic light is low, at most a few hundred photoelectrons per pixel per VIS exposure of 560 s, but still too much to meet the VIS noise requirements. It is very difficult to explain how this could occur, unless a misplacement of the MLI blankets has taken place at some time during the assembly or during the ascent phase. Alternatively, another option could be that a micro-meteoroid impact could have created a small protruding hole.

A weaker albeit still significant straylight component was measured for SAA~90 deg and AA < −6 deg. This corresponds to the rotation where the side of the spacecraft with the boom is in the shade, but where the other side is closer to the shadow edge of the sunshield. The most probable root cause for this secondary component is light diffraction by the side

edge of the sunshield towards an unprotected area of the MLI surrounding the PLM cavity. However also this is a speculation, as per design no unprotected area should be present.

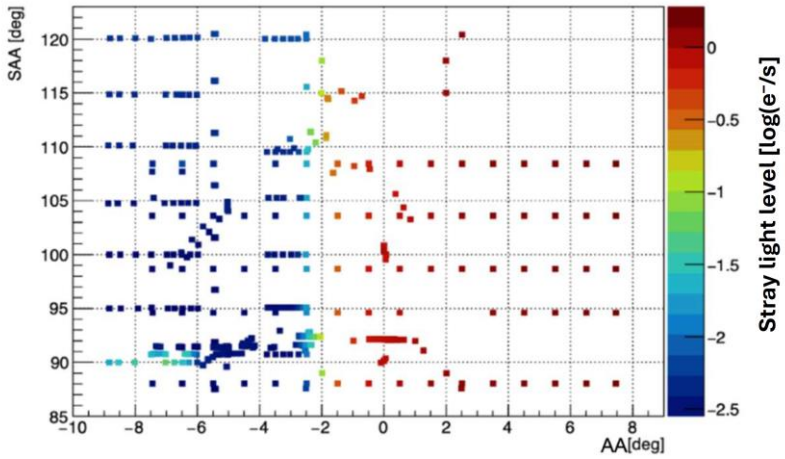

Figure 3: Parasitic straylight levels for different spacecraft attitudes with respect to the Sun obtained from VIS dark measurements with closed shutter. The colors indicate the average number of detected photoelectrons per VIS pixel per second. The finding was used to redefine the allowed SAA and AA angles for the Euclid wide survey. Credit: Euclid Consortium

Lesson learnt: unlike NISP, the VIS design consists of a number of separate elements (FPA, shutter and calibration unit) mounted in the PLM on the base plate, acting as optical bench. This open design with only MLI and partial baffles to ensure light tightness pose a risk for sensitive telescopes. The light tightness of the PLM was tested locally with lamps, which, in hindsight, were inadequate. . It is the question of whether the low observed levels of parasitic straylight could have been simulated and detected on ground with a proper test bench, like for example by a Solar simulation test.

6.2 Illumination of the VIS array by Solar X-rays

It was quickly noted that parts of the VIS focal plane array were affected by a higher density of glitches. At times the density became so high that clear patterns of bright pixels appeared. These patterns could be attributed to parts of the sunshield through which the Solar X-rays could pass. At high Solar activity an X-ray image of those parts of the sunshield could be detected by VIS, from which the direction and X-ray transparent parts of the sunshield could be inferred. Monitoring of the VIS images shows that high impact X-ray events are sporadic, and that only a fraction of the VIS image becomes unusable for scientific purposes. Less intense X-ray-events cause a higher glitch rate which can be removed by image processing to a high degree. The loss in the VIS area is estimated to be less than 3%. This is acceptable for the *Euclid* mission without further operational mitigation. It is also expected that the frequency of the events will drop with the passing of the Solar maximum predicted to peak in 2025.

Lesson learnt: during the development phase there were studies leading to shielding models to keep the dose of ionizing radiation on the detectors within the required level to ensure the end-of-life performance of the CCDs. This study was not specifically addressing the shielding for X-rays. X-ray radiation does not damage the detectors but does affect the scientific performance. The radiation analysis and design were performed also under the assumption – finally revealed to be wrong – that a sufficient shielding against ionizing radiation, dominated by Solar electrons, and non-ionizing radiation, dominated by the Solar protons and heavier ions, would also shield against X-ray radiation.

6.3 Fine guidance sensor (FGS) tracking anomaly

The FGS consists of two pairs of CCDs independently mounted on the sides of the VIS focal plane array. The CCDs are the same as the VIS CCDs but operated with different readout settings, it uses windowing and a much shorter exposure time. It was found that the FGS was not able to initiate and sometimes keep its guiding especially in regions of low stellar density. The root cause was an insufficient rejection of cosmic rays by the FGS causing the system to confuse these glitches with stellar images.

It was decided to update the FGS guiding software by employing two consecutive FGS exposures for the rejection of the glitches and other minor changes. The development, testing, and successful validation of the software took a few weeks to

complete. Following a thorough validation on ground, in the period from 18 September until 27 September the updated FGS software was tested in orbit by industry, and subsequently by tests planned by SOC involving observations defined by the instrument operation team and the SOC. The results of these tests showed that the new FGS software worked according to expectations and that the operations could be resumed; the measured pointing performance is illustrated in Fig. 4.

Lesson learnt: given the extremely high performance required by the FGS, compared to standard star trackers, the development of the FGS should have been considered as a separate instrument, rather than a standard SVM subsystem as part of the attitude and orbit control system (AOCS).

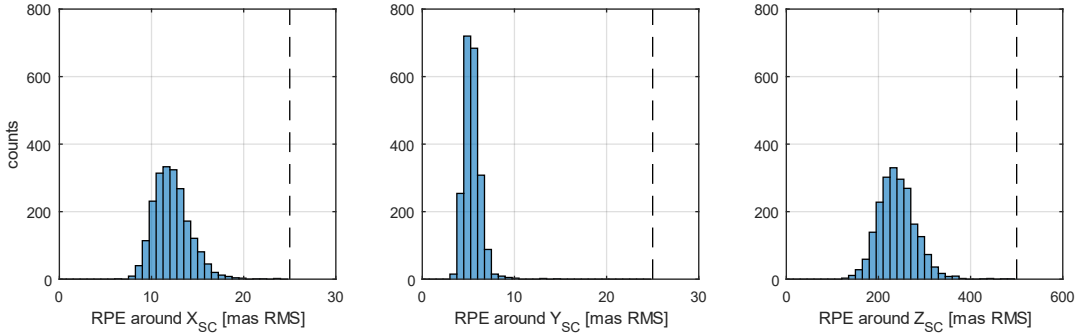

Figure 4: Relative Pointing Error (RPE) statistics for the three spacecraft rotations evaluated as RMS in mas during simultaneously collected VIS Nominal Science / NISP Spectroscopy exposures. The sample contains 2104 exposures taken in May 2024 after the FGS software update. The dashed lines indicate the allocation of the Euclid PSF shape requirements to the spacecraft pointing stability. Outliers where the tracking was lost are not included in the histograms, they amount to 1.5% of the exposures. One reference observing sequence (ROS) contains 4 VIS Nominal Science / NISP Spectroscopy exposures.

7. PERFORMANCE VERIFICATION (PV) PHASE

The PV Phase was planned to start right after the Spacecraft Commissioning Phase. While the spacecraft commissioning phase was meant to verify the in-flight performance of key subsystems in the SVM and PLM, the PV phase was devoted to the verification of the mission performance. This encompasses the flow-down of the budgeting, the instruments and payload calibration activities, and the assumptions on which the standard survey observations and the survey scanning strategy are based. An important PV phase objective is the detection of ice contamination. In-orbit information on the possible evolution of the contamination influences the timing and cadences of the routine calibration activities. The planning of the PV activities was guided by the calibration framework (CalF), a tool where sets of PV and routine (calibration) observations, the CalBlocks, and the resulting calibration information derived from the CalBlocks, the CalProducts, are described. The CalF considers the flow down of the calibration requirements and the accompanying budgeting. The modular and self-contained CalBlock approach together with multiple choices of suitable targets allows for a planning flexibility. During the PV phase, the operations planning procedure demands a minimum size of an uplink period of 1 week, meaning that the operations are executed autonomously by the spacecraft for at least one week.

The final PV plan consisted of 30 different CalBlocks. The plan included regular visits to the “self-calibration” field, which is an area of about 1 deg^2 close to the north Ecliptic pole (NEP). This location on the sky has perennial visibility and is therefore ideal for monitoring the photometric stability throughout the year, including the throughput in the bands as an indicator for ice contamination. The PV plan also included a 15-day period to qualify the phase-diversity calibration (PDC) procedure. The first 10 days of the PDC procedure were dedicated to monitoring the temperature stabilization of the system after a worst-case thermal disturbance induced by rotating the spacecraft from AA = −8.5 deg to AA = −3.5 deg while keeping SAA constant. During the 10-day period the attitude of the spacecraft with respect to the Sun was kept constant to avoid any thermal changes due to attitude changes to allow for a complete temperature stabilization at the end of the period.

From the start of the planned PV phase on 12 August 2023 until 18 September only a few good CalBlocks data could be collected. Activities were scheduled which were uncritical with respect to frequent guiding errors, which persisted in this early phase. This included straylight pointing scans to map the VIS straylight levels in the AA and SAA plane. The PV phase fully resumed on 30 September 2023. The first week of the PV restart was scheduled with caution, but the updated

FGS software showed a dramatically improved guiding performance allowing pointing-critical PV observations and PDC. The PV observations could be executed without major anomalies until 3 December 2023 within the originally allocated two months duration of PV.

Including the initial operations in August 2023 and interruptions to solve the guiding problems, the PV activities have lasted 113 days. About 7500 commanded pointings were executed and in total more than 12 000 VIS and 24 000 NISP exposures were collected. Despite the initial problems the execution of PV has been a huge success.

Lessons learnt: it was vital for the successful PV phase execution to have broken up the observations into smaller and self-contained blocks that could be re-arranged and repeated due to unforeseen events. Indeed, on day 1 of the scheduled PV period the carefully crafted pre-launch observing plan was no longer valid. Some observations had only single acceptable targets with limited visibility periods, which should have been avoided to make (re-)scheduling as flexible as possible.

8. PHASE DIVERSITY CALIBRATION (PDC) CAMPAIGN

The PDC campaign is part of the nominal mission to characterize the VIS PSF at any position in the VIS focal plane to determine the apparent shape of extended sources of 0.3 arcsec or larger. During the development of *Euclid* it was found that the model of the variation of the PSF as a function of spatial position and time could not be constructed on the basis of the wide survey exposures alone, because the available stars in the FoV provided insufficient signal to meet the required residual model uncertainty of $\sigma(e_i) < 2\times10^{-4}$ per ellipticity component with respect to the system PSF. Additional PSF knowledge had to be obtained to meet the required accuracy.

The VIS PSF depends on detector effects, guiding (i.e. spacecraft jitter) performance and the telescope optical path differences that are expected to vary with the thermo-elastic state of the spacecraft. With each pointing of the survey, the Sun is illuminating the satellite from a slightly different direction causing a thermo-elastic variation, thereby changing the position and shape of the telescope optical surfaces. These modulations result in a slightly different telescope for every exposure, and cause a spatial-temporal variation of the system PSF.

The overall thermo-elastic behavior on the image quality was studied by ESA and industry during the development phase before launch. The main results of this structural thermal and optical performance (STOP) analysis are reported in [23]. However, the analysis was limited to extreme “design cases” aimed to demonstrate that even during the worst possible temperature excursions the performance of the telescope in-orbit meets the image quality requirements.

The characterization or knowledge of the VIS PSF needs to be about two orders of magnitude better than the achieved hardware performance in terms of PSF FWHM, R^2 and ellipticity [3]. The aim of the PDC campaign is to build the in-orbit optical wavefront model of the telescope for a few thermal states represented by a set of spacecraft attitude (SAA and AA) combinations. Later in the PSF modelling process, this basis set will be used to fit the time-variable component of the wavefront error on science data. A precise wavefront retrieval aiming at a 1.0 nm optical path difference (OPD) can only be obtained by limiting the temperature disturbances to a much higher degree during the survey operations. The PDC thermal states were expected to be attained after a thermalization period of 7 days, which is several times the thermal time constant of the telescope components and the PLM Baseplate, sufficiently long for the system to reach a thermal equilibrium. The temperature evolution during the thermalization period was tested during the PV phase (Section 7).

Euclid has adopted the phase diversity method where the WFE is inferred by fitting in- and out-of-focus data. The PDC campaign consists of two kinds of observations:

- In-focus observations: deep high-signal to noise observations of dense stellar fields with the telescope in-focus.
- PDC observations: deep high-signal to noise observations of dense stellar fields with an extra-focused, focused, and intra-focused telescope. These were accomplished by setting the M2 focusing mechanism to +18 micron (extra-focus) and -18 micron (intra-focus) for the out-of-focus observations.

The frame exposure time for both kinds of observations was shorter than for the wide survey to obtain unsaturated detection of the brighter stars which will have lower peak brightness when out of focus. The observing period related to a given thermal state lasted 10 and 8 consecutive days for the PDC and in-focus observations, respectively, including the thermalization period.

During the thermalization periods the SAA and AA angles are fixed, but the spacecraft can still rotate around the Sun vector. Albeit in a highly constrained attitude condition, this gave us the opportunity to collect scientific observations by scheduling standard survey observations during these periods.

The PDC campaign started on 3 December 2023 and ended on 11 February 2024, enabling 7 thermal states, with 4 PDC observations including a high-polarization region, and 3 in-focus observations. Due to the required attitude constraints and limited amount of high-stellar density calibration fields, the scheduling and operation of these observations were highly customized. This had an impact on the SOC planning software, the a-priory selection of the spacecraft attitude in case of a safe-mode during thermalization periods, and the cadence of the satellite and orbit maintenance periods which were forced to be scheduled between the thermal states.

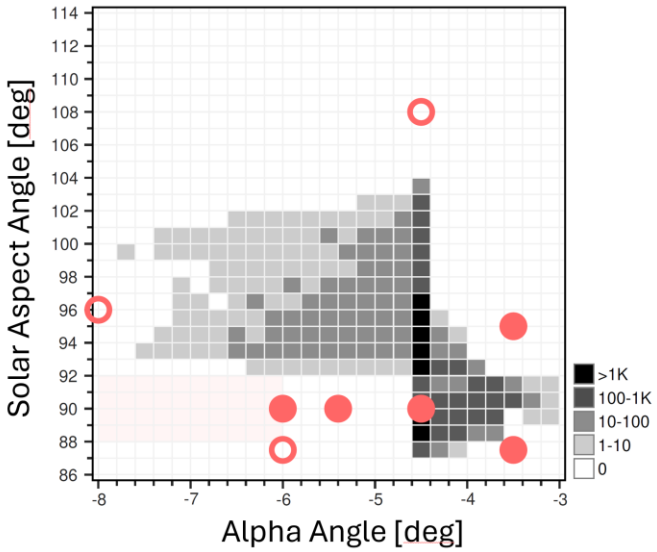

Figure 5: The base set of thermal states collected during the PV phase (at SAA=0, AA= –6) and PDC campaign. The filled red circles denote the SAA, AA positions of the PDC observations, the open circles give the in-focus observations. The grey squares indicate the frequency of SAA, AA combinations during the wide survey. Credit: J. Dinis on behalf of the Euclid Consortium

Analysis of the thermal data obtained during the demonstration PDC during PV phase showed that the thermal dissipation of both instruments significantly affected the temperature stability of the telescope. Temperature variations as small as 50 mK have a noticeable effect on the focus of the telescope. It was found that the VIS dissipation for the science observations executed during the thermalization periods had to be adjusted to match the dissipation during the in-focus and PDC observations. This was accomplished by including VIS short science exposures in all four dither pointings in the reference observing sequence (ROS) template. For the PDC observations it was decided to disable NISP during the preceding thermalization periods because idling NISP only just before the PDC observation would cause a disturbing drop in temperature during the PDC observation, which has a longer duration than the in-focus observation.

The final analysis of the PDC campaign data is ongoing and the application PSF / wavefront error model will be included in the WL shear processing function of the science ground segment.

9. SPECTROSCOPY PERFORMANCE

To cope with the confusion of the spectra in red channel ($1.25 < \lambda$ (micron) <1.85) of the NISP slitless spectrometer, spectra are taken with grisms RGS000 and RGS180, which are two separate grisms mounted in the grism wheel with 0 deg and 180 deg dispersion direction, respectively. By controlling the filter wheel rotation, these grisms are tilted by +4 deg for RGS000 and −4 deg for RGS180 to collect two additional spectrograms providing a total of 4 different dispersion directions for the spectral decontamination. Each dispersion direction must be calibrated separately, on top of the calibration of the blue grism BGS000 ($0.92 < \lambda$ (micron) < 1.30).

Observations obtained during the PV phase showed that the spectral response agrees with the expected response from ground tests [6], [16]. The detector quantum efficiencies were derived from ground calibrations. Since the QEs are better

than required, it was concluded that the required flux limit in the red NISP channel can be met, also for the ±4 deg tilted spectra where a few percent throughput loss is expected due to vignetting. The spectral resolution $R=\lambda/\Delta\lambda$ in the red grism RGS180 was measured from observations of emission lines in the spectra of a planetary nebula. The derived wavelength dispersion was R ~500 at 1.25 micron and increasing to R ~700 at the 1.85 micron long wavelength cut-off. These values are higher than the required minimum value of R = 380, which is advantageous. It is also found that the wavelength accuracy of the spectra is well within requirement. The observations during the early mission phases confirm the instrumental properties measured in-orbit are in line with the expectations based on the on-ground tests.

The success of the GC cosmological probe depends on the identification and redshift extraction of the Hα galaxies. This entails accurate calibration of the H2RG sensors [17] determination of the positions of the sources in the spectrograms, effective decontamination of the spectra, and extraction and identification of the spectral features. This is a complicated and difficult processing task by the SGS. During the first year of the *Euclid* mission a very pure galaxy sample will be collected by observing two deep fields at planned epochs to obtain a sufficient range of different grism rotations. This sample is required to determine the purity and completeness of the wide survey Hα galaxy detections, providing an assessment of the performance of the GC probe with *Euclid*.

10. ICE CONTAMINATION IN ORBIT

Based on predictions from industry, possible buildup of water ice on sensitive optical surfaces [22] was a big concern for *Euclid* before launch, given the large uncertainties on the quantitative effects of the ice on the optical parameters (image quality and photometry). The contamination would critically affect the PSF modelling, especially if deposited on complex coating surfaces such as the dichroic. Dedicated ice contamination observations at the same sky location were scheduled throughout the PV phase to track photometric changes through relative photometry on the same objects.

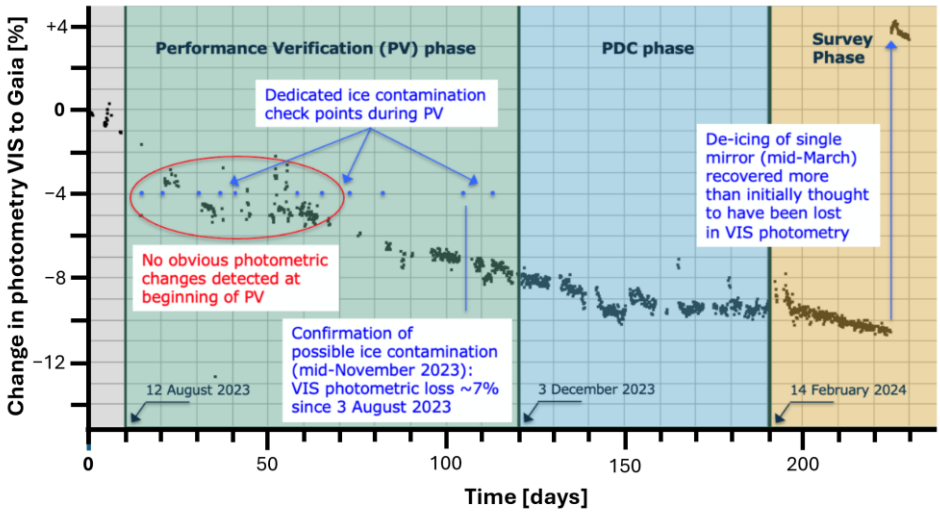

Figure 6: Adaptation of the analysis of VIS photometry provided by K. Kuijken against the Gaia DR3 catalogue throughout the PV phase and Early Science Operations phase. The throughput timeline was produced after the photometric losses in the VIS instrument became evident around mid-November 2023. The first de-icing campaign carried out in mid-March 2024 (day235) restored the VIS photometry to even higher levels than initially though. This result suggests stronger losses during the spacecraft commissioning phase than detected at the beginning of August 2023.

During the first half of the PV phase the analysis showed no obvious changes in photometry, which was a welcome surprise, which later - after also considering spacecraft commissioning data and using better calibrations - turned out to be a possible effect of the largely unknown and possibly highly non-linear relation of photometric losses with ice thickness on the mirrors.

At the time of confirmation of possible losses in VIS photometry around mid-November 2023, the accumulated loss had already reached about 7% with respect to the earliest data available from the spacecraft commissioning phase. There was a clear indication that only the VIS instrument was affected but not NISP. The root cause analysis narrowed the choice of possible contaminated surfaces to a single mirror, the last folding mirror in the optical path after the dichroic (FOM3) and

therefore only affecting VIS and not NISP. A specific procedure was therefore developed over the following weeks to selectively heat this mirror (and another one in the common optical path for confirmation) just above the water ice sublimation point in vacuum.

Even though the photometric losses seemed to settle at a constant 10-11% level, it was decided in February 2024 to activate the selective decontamination procedure. The result was a spectacular ~15% recovery in VIS photometry, more than expected based on the first available measurements from the spacecraft commissioning phase (Fig. 6). On the downside, the released amount of ice, possibly also on the support structures of the mirrors, might have caused cross-contamination to a common optical path element slightly affecting the NISP photometry after de-icing.

After this successful decontamination campaign, the throughput loss appeared again. A new selective decontamination campaign for the same mirror was done now in June 2024. While a detailed analysis is still outstanding, the first results are very promising again. A mission strategy with respect to decontamination must be derived based on the results of the first two initial campaigns to provide the best throughput of both instrument responses throughout the nominal survey.

Lessons learnt: the global decontamination procedure prepared pre-launch was suitable only right after launch. However, it would be very disruptive during science operations when all elements have already thermally stabilized and should only be considered as a last resort. Procedures for selective and controlled heating, and the monitoring of individual sensitive optical surfaces should be prepared before launch to allow for optimum mitigation against the unavoidable contamination with water ice.

11. ROUTINE SURVEY AND PLANNING STRATEGY

The *Euclid* survey consists of the following components: the wide survey, the deep survey and the routine calibrations. The wide and deep surveys are situated inside the region of interest (ROI), which is a 16 217 deg^2 area of extragalactic sky in which the required depth can be achieved for a single standard field observation or reference observing sequence (ROS) [18]. The ROI was updated in 2023 following the final survey plan by the Vera C. Rubin Observatory for the upcoming 10-year Legacy Survey of Space and Time (LSST). The ROI was optimized to maximize the overlap with LSST Wide Fast Deep area to 10 200 deg^2. It is expected that the depth of LSST will improve *Euclid's* dark energy figure of merit by more than 15%. Note that LSST has included the *Euclid* Deep Field South (EDFS) in their list of deep drilling fields. The EDFS stadium shape is mapped by two Rubin pointings: EDFS_a and EDFS_b [24].

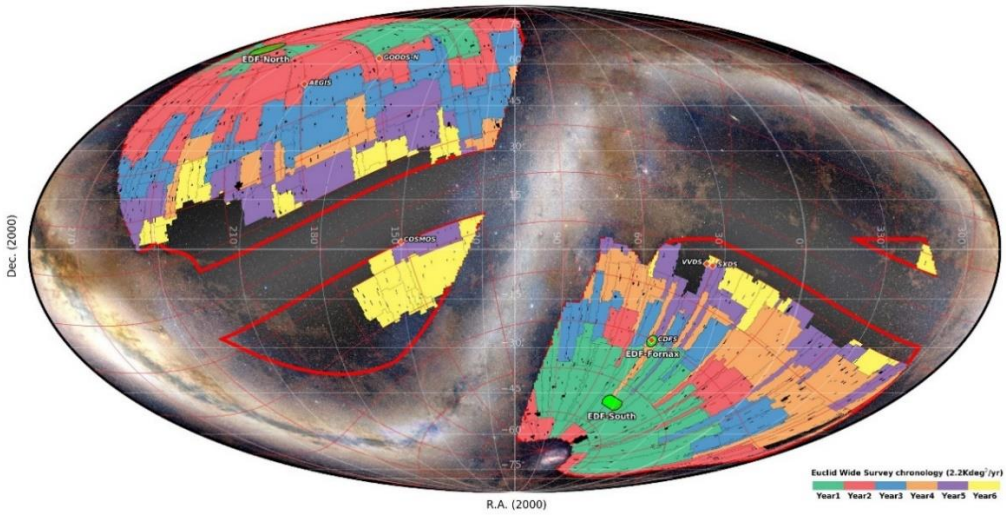

Figure 7: The Euclid survey coverage during the 6-year nominal mission in equatorial coordinate frame. The survey plan RSD2024A was delivered for operation to ESA in January 2024. The red borders delineate the region of interest (ROI), which was optimized to maximize the overlap with LSST. In the first year of the survey, scheduling priority is given to the southern hemisphere to maximize the overlap with the Dark Energy Survey, which data are used for DR1. The northern hemisphere ground-based data are provided by the Ultraviolet Near-Infrared Optical Northen Survey (UNIONS) consortium, covering declinations above +15 deg. Credit: Survey Operations Support Team on behalf of the Euclid Consortium.

The ROS observing sequence was tested on-ground and was also validated during the spacecraft commissioning phase. Marginal timing changes had to be introduced to accommodate for AOCS updates associated with the filter wheel compensating mechanism. Including adjustments to the slew time allocation, the in-orbit ROS duration increased by 38 s compared to the pre-launch value. This, however, had little impact on the survey performance.

The new SAA and AA constraints to minimize the parasitic straylight level imposed a smaller available AA range which caused a major replanning of the survey. The updated survey plan (RSD2024A) requires more overlap between the fields to fill the area, causing a decrease of the total area that can be achieved during the 6-year nominal mission to 13,400 deg^2 which is below the required survey area of 14 000 deg^2. Note that this mission requirement was adopted before launch and is lower than the initial science requirement of 15 000 deg^2 given in [2]. It is predicted that the required area can be completed with an additional 4 months of mission time. In view of the operational uncertainties during the nominal mission, it was decided to accept the RSD2024A survey plan.

12. THE EARLY RELEASE OBSERVATIONS (ERO) PROGRAM

The *Euclid* ERO program was introduced by the Euclid Science Team to obtain scientific observations for communication and outreach purposes as well as early scientific results before the start of the nominal mission. The program could make full advantage of the scheduling flexibility during the early mission phases; this flexibility has not been included in the design of the routine survey operations. A total of one day (about 24 hours) of observing time was allocated for the collection of captivating deep-sky fields with interesting science cases that are outside the scope of the core-cosmology objectives. Based on a pre-launch call to the Euclid Collaboration, the ERO program committee selected 6 proposals, which together cover a range of astronomical scales and showcasing the diversity of science cases offered by the *Euclid* data. The ERO program required the usage of the ROS observing template [18], which facilitates the planning, scheduling, and the early calibrations of the proposed fields. Most observations were taken during the PV phase in October and November 2023, but a few of them were obtained before that period enabling a first assessment of the scientific performance of the ROS. Two proposals requested a higher field depth with respect to the predicted survey depth. For these cases more than one ROS per field was scheduled with an offset of a few arcminutes between the ROS pointings to homogenize the stacked coverage of the VIS and NISP detectors. The ERO data were processed with a dedicated pipeline containing already available routines building on the large existing expertise acquired from ground- and space-based imaging, photometry, and astrometry with CCD and H2RG sensors.

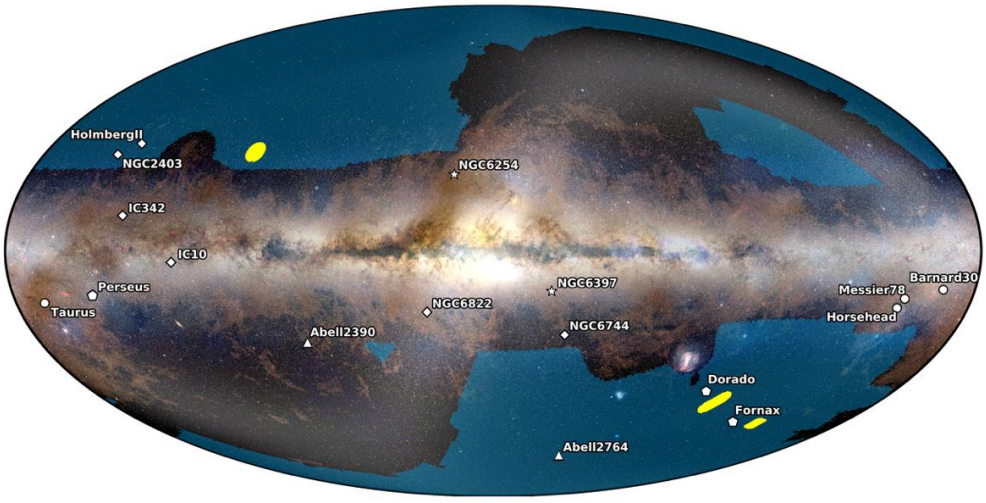

Figure 8: Distribution on the sky in Galactic coordinate frame of the 17 ERO targets, which have their data released to the public on 23 May 2024. The Euclid survey is given in blue, the yellow areas are the Euclid deep fields. The ERO observations were not confined to the ROI defined by the core science program of Euclid, stressing the legacy (i.e. non-core-science) value of the ERO observations. The targets Fornax, IC10, Taurus, Perseus and NGC2403 were obtained during the anomalous guiding period, see Fig. 1. The large spread of ERO positions reflects the long period of target collection from early September to the end of November 2023. Courtesy: J.-C. Cuillandre on behalf of the Euclid Consortium.

The ERO program released its first results to the public in November 2023 demonstrating the power of the combination of large field of view, high spatial resolution, and depth in the visual and near-infrared *Euclid* bands. Taking the median values over all fields, the ERO program achieved a 10 σ detection limit for galaxies (small extended sources) of 25.3 AB mag in VIS and 23.0 AB mag or better in the NISP bands, and 5 σ detection limit for point sources of 27.1 AB mag in VIS and 24.5 AB mag or better in the NISP bands [20]. These values comply with the required detection limits of 24.5 AB mag (10 σ) for extended sources in VIS and 24 AB mag (5 σ) for point sources in the NISP bands [2]. In addition, the measured low surface brightness (LSB) median performance of better than 29.9 AB mag arcsec^{-2} in VIS and 28.2 mag arcsec^{-2} in NISP for the single ROS observations demonstrates the effectiveness of the straylight suppression [8][21], which include the continuous care in handling the environment until moments before launch. The LSB performance enables an additional powerful scientific capability with *Euclid*. We note that these photometric measurements were taken at the earliest mission phases, they may not be fully representative for the survey observations where temporary throughput losses due to ice could degrade the detection limits. The astrometry is better than 10 mas with VIS, and more than half of the fields have an astrometric performance of better than 5 mas with VIS.

Figure 9: Color composite image from the VIS, NISP Y, and H bands of one ROS observation of 70 minutes of the Horsehead Nebula. The image demonstrates the combination of wide field, diffraction limited resolution, depth, and dynamic range in the optical and near-infrared bands. Credit: ESA/Euclid/Euclid Consortium/NASA, Processing: J.-C. Cuillandre (CEA Paris-Saclay), G. Anselmi

A total of 17 fields were observed and the scientific data (stacked images and catalogues) were released to the public [25] in May 2024. At the same time, a first set of 10 showcasing papers were published in ArXiv and submitted for peer review

publication. These papers are part of the scientific validation of the data. A detailed description of the ERO program, the image processing pipeline, and the instrumental performance assessment are presented in [20].

The ERO program has also collected spectroscopic exposures, which are part of the ROS template. These observations require dedicated *Euclid* calibrations and processing routines which were not available. The processed spectroscopy data will be made available at the first data release (DR1), which is currently scheduled for June 2026.

13. OUTLOOK

The first year of *Euclid* operations has given us the confidence that the *Euclid* mission can fulfill its scientific objectives. The telescope assembly and instruments are performing according to specifications. This is supported by the results of the ERO program for imaging with VIS and NISP. The unexpected in-obit anomalies which could have an impact on the scientific performance were mitigated. Due to the presence of parasitic straylight, the reprogramming of the survey plan has led to a smaller total survey area than required, equivalent to a loss of 4 months survey time over a 6-year mission. The mission limiting consumable is the supply of cold gas. Measurements taken by the flight control team and industry after PV phase suggest a comfortable margin for extended operations significantly beyond 7 years.

For *Euclid's* core cosmology, the construction of the PSF model including the PDC campaign results to achieve the accuracies demanded by the WL probe is a major challenge. Likewise, meeting the purity and completeness requirements for the CG probe requires the completion of the dedicated NISP grism calibration observations and substantial spectroscopy data processing and analysis efforts.

A major challenge will also be the storage, distribution and analysis of the vast volume of data generated by the mission. *Euclid* generates some 100 Gbyte of compressed raw science data per day, and a multitude of this volume is generated by the SGS in pixel data products and catalogs. A dedicated data platform (datalabs) is under development by ESA.

The activities are driven by the public data release plan, approved by the ESA science program committee. The first "quick" data release Q1 covers a survey area of 53 deg^2 and is planned for March 2025. Based on the success of the ERO program, we can expect a high legacy science return. The first cosmology data release (DR1) contains 1 year of survey products (covering some 2300 deg^2) and is planned for June 2026. DR2 and DR3 are planned 2 and 5 years after DR1, with in between 3 Q releases on an annual basis.

ACKNOWLEDGEMENTS

The Euclid Consortium acknowledges the European Space Agency and a number of agencies and institutes that have supported the development of *Euclid*, in particular the Agenzia Spaziale Italiana, the Austrian Forschungsförderungs-gesellschaft funded through BMK, the Belgian Science Policy, the Canadian Euclid Consortium, the Deutsches Zentrum für Luft- und Raumfahrt, the DTU Space and the Niels Bohr Institute in Denmark, the French Centre National d'Etudes Spatiales, the Fundação para a Ciência e a Tecnologia, the Hungarian Academy of Sciences, the Ministerio de Ciencia, Innovación y Universidades, the National Aeronautics and Space Administration, the National Astronomical Observatory of Japan, the Netherlandse Onderzoekschool Voor Astronomie, the Norwegian Space Agency, the Research Council of Finland, the Romanian Space Agency, the State Secretariat for Education, Research, and Innovation (SERI) at the Swiss Space Office (SSO), and the United Kingdom Space Agency. A complete and detailed list is available on the Euclid website (http://www.euclid-ec.org).

REFERENCES

[1] Albrecht, A., Bernstein, G., Cahn, R., et al., "Report of the Dark Energy Task Force", arXiv: astro-ph/0609591 (2006)
[2] Laureijs, R., Amiaux, J., Arduini, S., et al., "Euclid Definition Study Report", arXiv:1110.3193 (2011)
[3] Euclid Collaboration: Mellier, Y., Abdurro'uf, Acevedo Barrosoet, J. A., et al., "Euclid. I. Overview of the Euclid mission", arXiv:2405.13491 (2024)
[4] Racca, G.D., Laureijs, R., Stagnaro, L., et al, "The Euclid mission design", Proc. of SPIE Vol. 9904, 99040O (2016)

[5] Euclid Collaboration: Cropper, M., Al-Bahlawan, A., Amiaux, et al., "Euclid. II. The VIS Instrument", arXiv:2405.13492 (2024)
[6] Euclid Collaboration: Jahnke, K., Gillard, W., Schirmer, M., et al., "Euclid. III. The NISP Instrument", arXiv:2405.13493 (2024)
[7] Laureijs, R., Racca, G.D., Mellier, Y., et al., "Euclid Mission Status after Mission Critical Design", Proc. of SPIE Vol. 11443, 114430F (2020)
[8] Gaspar Venancio, L.-M., Carminati, L., Amiaux, J, et al., "Status of the performance of the Euclid spacecraft", Proc. of SPIE Vol. 11443, 114430G (2020)
[9] Bougoin M., Mallet, F., Lavenac, J., et al., "Full-SiC EUCLID's very large telescope", Proc. of SPIE Vol. 11180, 111801P (2018)
[10] Endicott, J, Darby, S., S. Bowring, S., et al., "Charge-Coupled Devices for the ESA Euclid M-class Mission", Proc. of SPIE Vol. 8453, 845304 (2012)
[11] Prod'homme, T., Verhoeve. P., Kohley, et al., "A comparative study of charge transfer inefficiency value and trap parameter determination techniques making use of an irradiated ESA-Euclid prototype CCD" Proc. of SPIE Vol. 9154, 915409 (2014)
[12] Szafraniec, M., Azzollini, R., Cropper, M., et al., "On-ground characterization of the Euclid's CCD273-based readout chain", Proc. of SPIE Vol. 9915, 991510 (2016)
[13] Waczynski, A., Barbier, R., Cagiano, S., et al., "Performance Overview of the Euclid Infrared Focal Plane Detector Subsystems" Proc. of SPIE Vol. 9915, 991511, (2016)
[14] Gaspar Venancio, L., Carminati, L., Lorenzo Alvarez, J., et al., "Coating induced phase shift and impact on Euclid imaging performance", Proc. of SPIE Vol. 9904, 99040V (2016)
[15] Baron, M., Sassolas, B., Frugier, P.-A., et al., "Measurement and modelling of the chromatic dependence of a reflected wavefront on the Euclid space telescope dichroic mirror", Proc. of SPIE Vol. 12180, 121804V (2022)
[16] Medinaceli, E., Valenziano, L., Auricchio, N., et al., "EUCLID's Near Infrared Spectro-Photometer ready for flight- review of final performances", Proc. of SPIE Vol. 12180, 121801L (2022)
[17] Barbier, R., Buton, C., Clemens, J.-C., et al., "Detector chain calibration strategy for the Euclid Flight IR H2RGs", Proc. of SPIE Vol. 10709, 107090S (2018)
[18] Euclid Collaboration: Scaramella, R., Amiaux, J., Mellier, Y., et al., "Euclid preparation. I. The Euclid Wide Survey", A&A, 662, 112 (2022)
[19] Gaspar Venancio, L., Laureijs, R., Racca, G., et al., "An account of the Euclid payload module test results", Proc. of SPIE Vol. 12777, 127776H (2022)
[20] Cuillandre, J.-C., Bertin, E., Bolzonella, et al., "Euclid: Early Release Observations -- Programme overview and pipeline for compact- and diffuse-emission photometry", arXiv:2405.13496 (2024)
[21] Gaspar Venancio, L.-M, , Pachot, C., Carminati, L., et al., "Euclid end-to-end straylight performance assessment", Proc. of SPIE Vol. 9904, 99040P (2016)
[22] Euclid Collaboration: Schirmer, M., Thürmer, K., Bras, B., et al., "Euclid preparation. XXIX. Water ice in spacecraft Part 1: The physics of ice formation and contamination", A&A 675, 142 (2023)
[23] Anselmi et al. (2024), *in preparation*
[24] LSST survey strategy, see: https://survey-strategy.lsst.io/baseline/ddf.html
[25] ERO data products are downloadable from https://www.cosmos.esa.int/web/euclid/ero-public-release